LETTER

doi:10.1038/nature09718

Grains and grain boundaries in single-layer graphene atomic patchwork quilts

Pinshane Y. Huang[1]*, Carlos S. Ruiz-Vargas[1]*, Arend M. van der Zande[2]*, William S. Whitney[2], Mark P. Levendorf[3], Joshua W. Kevek[4], Shivank Garg[3], Jonathan S. Alden[1], Caleb J. Hustedt[5], Ye Zhu[1], Jiwoong Park[3,6], Paul L. McEuen[2,6] & David A. Muller[1,6]

The properties of polycrystalline materials are often dominated by the size of their grains and by the atomic structure of their grain boundaries. These effects should be especially pronounced in two-dimensional materials, where even a line defect can divide and disrupt a crystal. These issues take on practical significance in graphene, which is a hexagonal, two-dimensional crystal of carbon atoms. Single-atom-thick graphene sheets can now be produced by chemical vapour deposition[1–3] on scales of up to metres[4], making their polycrystallinity almost unavoidable. Theoretically, graphene grain boundaries are predicted to have distinct electronic[5–8], magnetic[9], chemical[10] and mechanical[11–13] properties that strongly depend on their atomic arrangement. Yet because of the five-order-of-magnitude size difference between grains and the atoms at grain boundaries, few experiments have fully explored the graphene grain structure. Here we use a combination of old and new transmission electron microscopy techniques to bridge these length scales. Using atomic-resolution imaging, we determine the location and identity of every atom at a grain boundary and find that different grains stitch together predominantly through pentagon–heptagon pairs. Rather than individually imaging the several billion atoms in each grain, we use diffraction-filtered imaging[14] to rapidly map the location, orientation and shape of several hundred grains and boundaries, where only a handful have been previously reported[15–19]. The resulting images reveal an unexpectedly small and intricate patchwork of grains connected by tilt boundaries. By correlating grain imaging with scanning probe and transport measurements, we show that these grain boundaries severely weaken the mechanical strength of graphene membranes but do not as drastically alter their electrical properties. These techniques open a new window for studies on the structure, properties and control of grains and grain boundaries in graphene and other two-dimensional materials.

Figure 1a shows a large array of the suspended, single-layer graphene membranes used in this study. We grew predominately single-layer graphene films on copper foils by chemical vapour deposition[1] (CVD) using three different growth recipes, which we refer to as growth methods A, B and C. Unless otherwise stated, all data were taken on graphene grown with method A, which was similar to the recipe reported in ref. 1. Methods B and C are slight variations: method B uses ultrapure copper foils[18] (99.999% pure rather than 99.8%) and method C uses a rapid thermal processor furnace (Methods). These films were transferred onto holey silicon nitride or Quantifoil transmission electron microscopy (TEM) grids using two different techniques (Methods and Supplementary Information). One key innovation over previous graphene TEM sample fabrication[20] was the gentle transfer of the graphene onto a TEM grid using a minimum of polymer support and baking the samples in air to remove the polymer without liquid solvents. This produces large arrays of free-standing graphene sheets covering up to 90% of the TEM grid holes.

To characterize these membranes at the atomic scale, we used aberration-corrected annular dark-field scanning transmission electron microscopy (ADF-STEM), where a 60-keV, ångström-scale electron beam is scanned over the sample while the medium- to high-angle scattered electrons are collected. Keeping the electron beam voltage below the ~100-keV graphene damage threshold was necessary to limit beam-induced damage. Properly calibrated, this technique images the location and atomic number[21] of each atom and, along with TEM, has been used to study the lattice and atomic defects of graphene and boron nitrene[19,21–23]. Figure 1b shows an ADF-STEM image of the crystal lattice within a single graphene grain. Away from the grain boundaries, such regions are defect free.

In Fig. 1c, two graphene grains meet with a relative misorientation of 27°, forming a tilt boundary. Additional images of grain boundaries are shown in Supplementary Figs 2c and 3. As highlighted in Fig. 1d, the two crystals are stitched together by a series of pentagons, heptagons and distorted hexagons. The grain boundary is not straight, and the defects along the boundary are not periodic. Although the boundary dislocation

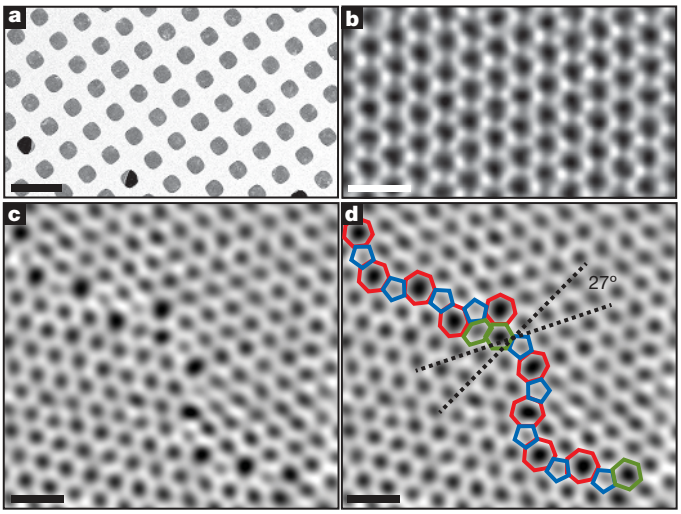

Figure 1 | Atomic-resolution ADF-STEM images of graphene crystals. **a**, Scanning electron microscope image of graphene transferred onto a TEM grid with over 90% coverage using novel, high-yield methods. Scale bar, 5 μm. **b**, ADF-STEM image showing the defect-free hexagonal lattice inside a graphene grain. **c**, Two grains (bottom left, top right) intersect with a 27° relative rotation. An aperiodic line of defects stitches the two grains together. **d**, The image from **c** with the pentagons (blue), heptagons (red) and distorted hexagons (green) of the grain boundary outlined. **b**–**d** were low-pass-filtered to remove noise; scale bars, 5 Å.

[1]School of Applied and Engineering Physics, Cornell University, Ithaca, New York 14853, USA. [2]Department of Physics, Cornell University, Ithaca, New York 14853, USA. [3]Department of Chemistry and Chemical Biology, Cornell University, Ithaca, New York 14853, USA. [4]Department of Physics, Oregon State University, Corvallis, Oregon 97331, USA. [5]Department of Physics and Astronomy, Brigham Young University, Provo, Utah 84602, USA. [6]Kavli Institute at Cornell for Nanoscale Science, Ithaca, New York 14853, USA.
*These authors contributed equally to this work.

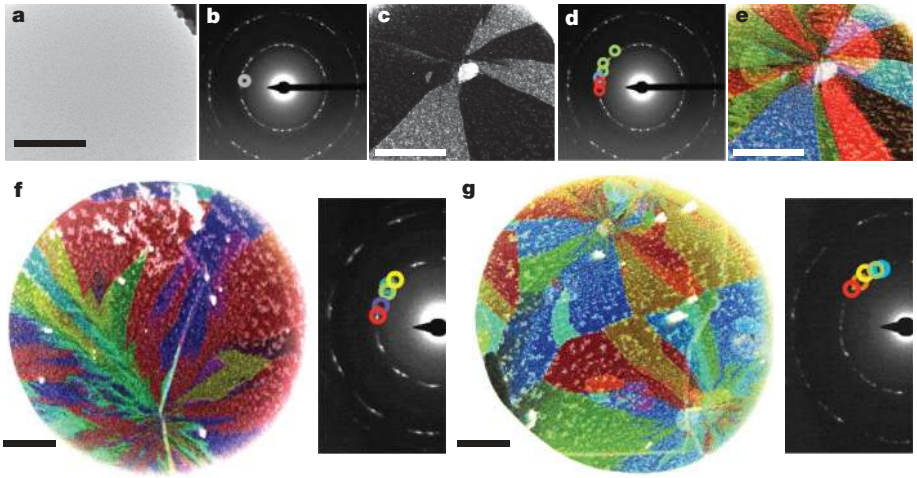

Figure 2 | Large-scale grain imaging using DF-TEM. **a**–**e**, Grain imaging process. **a**, Samples appear uniform in bright-field TEM images. **b**, Diffraction pattern taken from a region in **a** reveals that this area is polycrystalline. Placing an aperture in the diffraction plane filters the scattered electrons forming **c**, a corresponding dark-field image showing the real-space shape of these grains. **d**, Using several different aperture locations and colour-coding them produces **e**, a false-colour, dark-field image overlay depicting the shapes and lattice orientations of several grains. **f**, **g**, Images of regions where many grains emanate from a few points. Scale bars, 500 nm.

resembles structures proposed theoretically[11,13], its aperiodicity contrasts with many of these models and will strongly affect the predicted properties of grain boundaries. By analysing atomic scattering intensities[21], we confirm that the boundary is composed entirely of carbon. In addition, although high electron beam doses could induce isolated bond rotations (Supplementary Fig. 3), the boundary was largely stable under the 60-keV electron beam. Thus, the polycrystalline graphene is a strongly bonded, continuous carbon membrane. We also note that many grain boundaries are decorated by lines of surface particles and adsorbates (Supplementary Fig. 4), suggesting that, as predicted[10], they may be more chemically reactive than the pristine graphene lattice.

Both STEM and TEM, which determine the positions and identities of atomic nuclei, and complementary scanning tunnelling microscopy, used to probe valence wavefunctions[15–17], are invaluable for understanding the local properties of grain boundaries. Using these atomic-resolution approaches, however, tens of billions to hundreds of billions of pixels would be needed to image even a single micrometre-scale grain fully, with estimated acquisition times of a day or more. Other candidates for characterizing grains on larger scales, such as low-energy electron microscopy[18] and Raman microscopy[3], typically cannot resolve small grains and may be difficult to interpret. Fortunately, electron microscopy offers an ideal technique for imaging grains on the necessary length scales: dark-field TEM (DF-TEM), which is a high-throughput, diffraction-sensitive imaging technique[14] that can be implemented on most TEMs built in the past sixty years. This method is usually applied to foils about 100–300-nm thick[14], but we demonstrate below that, remarkably, it also works on single-atom-thick sheets—even on samples too dirty for atomic-resolution imaging. In this manner, DF-TEM provides a nanometre- to micrometre-scale grain analysis that complements ADF-STEM to give a complete understanding of graphene grains on every relevant length scale.

Figure 2a, b shows a bright-field TEM image of a graphene sheet along with the selected-area electron diffraction pattern created from this region of the membrane. Owing to graphene's six-fold symmetry, electron diffraction from a single graphene crystal results in one set of six-fold-symmetric spots. Figure 2b contains many such families of spots, indicating that the field of view contains several grains of different orientations. DF-TEM images these grains one by one with few-nanometre resolution using an objective aperture filter in the back focal plane to collect electrons diffracted through a small range of angles, as shown by the circle in Fig. 2b. The resulting real-space image (Fig. 2c) shows only the grains corresponding to these selected in-plane lattice orientations and requires only a few seconds to acquire. By repeating this process using several different aperture filters, then colouring and overlaying these dark-field images (Fig. 2d, e), we create complete maps of the graphene grain structure, colour-coded by lattice orientation, as shown in Fig. 2e–g.

The images obtained are striking. The grains have complex shapes and many different crystal orientations. In Fig. 2e–g, we observe special locations from which many grains emanate. Small particles and multilayer graphene also are often found near these sites; see, for example, Fig. 2e, top right. Both the average spacing (2–4 μm) and shapes of these radiant sites when we use growth method A are comparable with Raman and scanning electron microscope observations of graphene nucleation[1,3], suggesting that these locations are probably nucleation sites. Similar structures have been observed in studies of crystallization in colloids and are consistent with crystallization around impurities[24]. Similar multigrain nucleation on copper has recently been observed using low-energy electron microscopy[18]. Significantly, each apparent nucleation site gives rise to many grains of different orientations, resulting in a mean grain size much smaller than the nucleation density.

The distributions of grain size and relative angular orientation are readily determined from DF-TEM images. As discussed below, grain sizes are dependent on growth conditions, here ranging from hundreds of nanometres to tens of micrometres for slight changes in growth conditions. In Fig. 3a, we plot a histogram of grain sizes across several samples grown using method A. The mean grain size, defined as the square root of the grain area, is 250 ± 11 nm (s.e.m.). This size is much smaller than the grain size of the copper substrate[1,4] (100 μm–1 mm) and typical lateral grains measured in bulk, highly ordered pyrolytic graphite[25] (6–30 μm). The inset in Fig. 3a shows the cumulative probability of finding multiple grains in a given area. This plot demonstrates that micrometre-scale CVD graphene devices produced from this set of films will nearly always contain multiple grains. Figure 3b shows a histogram of the relative crystallographic angles between adjacent grains. Because of graphene's six-fold crystal symmetry, the diffractive imaging technique only determines grain rotations modulo 60°. Consequently, the measurable difference between grain orientations is from 0 to 30° (with, for example, 31° measured as 29°). We observe a surprising and robust preference for low-angle (~7°) grain boundaries and high-angle (~30°) boundaries similar to that seen in Fig. 1.

Additional information about these orientations comes from the larger-area diffraction patterns in Fig. 3c, which we created by averaging diffraction data sampled across 1,200-μm^2 regions of graphene. The broadened diffraction peaks in Fig. 3c (left) show a distinct six-fold pattern, indicating that a significant fraction of the grains are approximately aligned across large areas This alignment can also be seen in Fig. 3d, which is a low-magnification DF-TEM image showing grains with a small (~10°) range of in-plane lattice orientations. Almost half of the membrane appears bright, indicating that these grains are all approximately aligned. In contrast, a dark-field image of randomly oriented grains would only show roughly one-sixth (10°/60°) of the graphene membrane. In the diffraction pattern of a separately grown sample (Fig. 3c, right), we instead find a clear 12-fold periodicity,

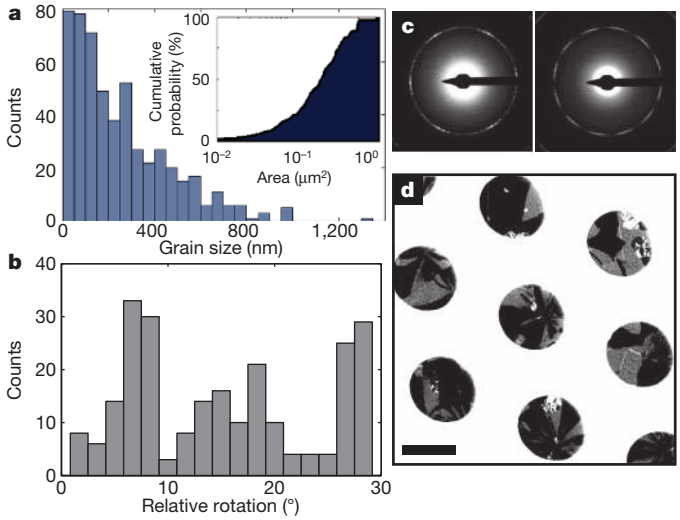

Figure 3 | Statistical analysis of grain size and orientation. **a**, Histogram of grain sizes, taken from three representative samples using DF-TEM. The mean grain size is 250 ± 11 nm (s.e.m., $n = 535$). Inset, plot of the cumulative probability of having more than one grain given the area of a device. **b**, Histogram of relative grain rotation angles measured from 238 grain boundaries. **c**, **d**, Large-area diffraction patterns (**c**) and a low-magnification DF-TEM image (**d**) show that grains are globally aligned near particular directions. Scale bar, 2 μm.

indicating that there are two main families of grains rotated from one another by 30°. These distributions, which often contain smaller subpeaks (Supplementary Fig. 6), are consistent with the frequent observation of low-angle and high-angle (~30°) grain boundaries. We attribute these alignments to registry to the copper substrate used for graphene growth. Such registry has recently been observed in low-energy electron microscopy and scanning tunnelling microscopy studies of graphene growth on copper (100) and (111) surfaces[15,16,18].

By directly correlating grain structure with growth methods, these DF-TEM methods can be used to build on recent studies[3] that have demonstrated links between island nucleation density and growth conditions. Fig. 4a–c shows three composite DF-TEM images of graphene grown using methods A, B and C. The slight differences between growth methods effected significant changes in the grain size, shape and crystallographic orientation of the CVD graphene. For example, with growth method C we observed grains averaging 1–4 μm (Fig. 4c), which is an order of magnitude larger than the grains grown using method A. Our DF-TEM methods provide a powerful characterization tool for understanding and controlling grain growth, which will be a rich field of study important for graphene applications.

The ability to image the grain structure in graphene monolayers easily opens the door to the systematic exploration of the effects of grain structure on the physical, chemical, optical and electronic properties of graphene membranes. We find that such studies are further facilitated because grain boundaries are visible in scanning electron microscopy and atomic force microscopy (AFM) phase imaging owing to preferential decoration of the grain boundaries with surface contamination (Fig. 5a and Supplementary Figs 9 and 10). Below, we show two examples probing the electrical and mechanical properties of grain boundaries.

We first examine the failure strength of the polycrystalline CVD graphene membranes (growth method A) using AFM. We used AFM phase imaging to image grains (Fig. 5a) and then pressed downwards with the AFM tip to test the mechanical strength of the membranes. As seen in Fig. 5b, the graphene tears along the grain boundaries. From repeated measurements, we find that failure occurs at loads of ~100 nN, which is an order of magnitude lower than typical fracture loads of 1.7 μN reported for single-crystal exfoliated graphene[26]. Thus, the strength of polycrystalline graphene is dominated by its grain boundaries.

We probed the electrical properties of polycrystalline graphene by fabricating electrically contacted devices using graphene from all three growth methods. Figure 4d shows a histogram of mobilities extracted from four-point transport measurements. Devices grown using methods A, B and C have room-temperature mobilities of 1,000 ± 750, 7,300 ± 1,100 and 5,300 ± 2,300 $cm^2 V^{-1} s^{-1}$(s.d.), respectively. The mobilities for growth method A are comparable to previous results on CVD graphene[1], whereas the mobilities of growth methods B and C are closer to those reported for exfoliated graphene[27] (1,000–20,000 $cm^2 V^{-1} s^{-1}$). By comparing these measurements with the corresponding DF-TEM images in Fig. 4a–c, we are surprised to find that, although mobility is clearly affected by growth conditions, high mobility does not directly correlate with large grain size.

To complement these bulk electrical measurements, we used scanning probe a.c. electrostatic force microscopy[28] (AC-EFM) to test the resistivity of individual grain boundaries. We fabricated suspended graphene membrane devices[29]. One of these is shown schematically in Fig. 5c, where we also plot the relative potential along a graphene membrane between two biased electrodes, measured using AC-EFM. In this plot, high-resistance grain boundaries would manifest as sharp drops in potential. The graphene in these devices (growth method A) had a mean grain size of 250 nm, so a line scan across these 3-μm-long membranes should cross an average of 12 grains. However, no noticeable potential drops were detected, indicating that most grain boundaries in these devices are not strongly resistive interfaces. By assuming that the grain boundary runs perpendicular to the line scan, we estimate an upper bound on the grain boundary resistance of $R_{GB} < 60\ \Omega\ \mu m/L$, where L is the length of the grain boundary, to be compared with the sheet resistance of $R_{graphene} = 700\ \Omega/\square$ for the entire device. In other words, the resistance of the grain boundaries is less than one-third the resistance of a 250-nm grain. Further measurements on six additional graphene membranes, both suspended and unsuspended, and from different growth methods, produced similar results. This small impact of grain boundaries stands in stark contrast to other materials, such as complex oxides, where a single grain boundary can lead to a million-fold increase in resistance over single crystals[30].

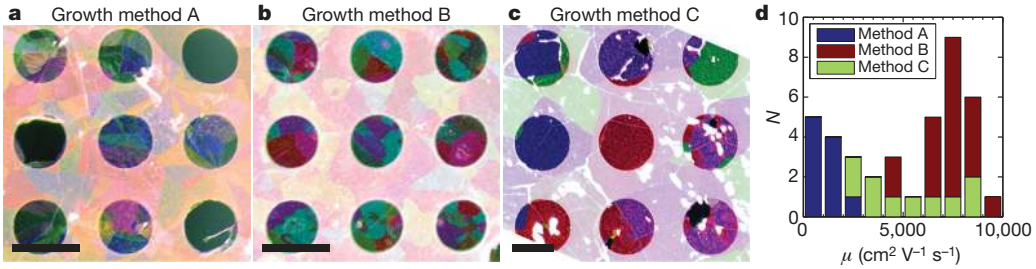

Figure 4 | Grain structure and mobilities for three growth conditions. **a–c**, Composite DF-TEM images of grain structure show variations with growth condition. The mean grain sizes are 250 ± 11 nm (s.e.m.; growth method A, 99.8% pure copper), 470 ± 36 nm (s.e.m.; growth method B, 99.999% pure (ultrapure) copper) and 1.7 ± 0.15 μm (s.e.m.; growth method C (rapid thermal anneal)). The graphene is visible through the 20-nm, perforated amorphous-carbon Quantifoil support film. The graphene is broken over three of the perforations in **a**. Scale bars, 2 μm. **d**, Vertically stacked histogram of room-temperature mobilities, μ, measured from 39 devices using graphene growth methods A, B, and C. N, number of devices. See Methods for further details.

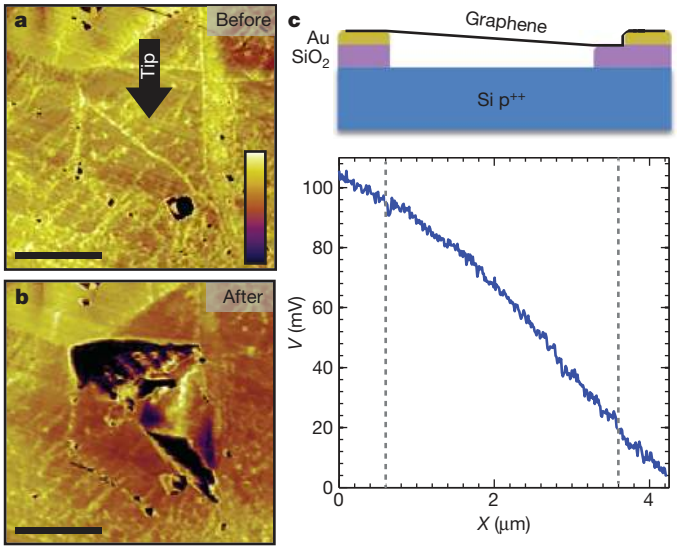

Figure 5 | AFM indentation and AC-EFM studies of graphene grain boundaries. **a**, **b**, AFM phase images of a graphene grain before and after an indentation measurement. **a**, Indentation takes place at the centre of this grain as shown by the arrow. **b**, The region is torn along grain boundaries after indentation. Scale bars, 200 nm. **c**, Electrostatic potential, averaged over three adjacent line scans along a suspended graphene sheet between two electrodes (schematic at top) and measured using AC-EFM. Although on average each line scan should cross 12 grains, no measureable features are present. Dashed lines indicate the locations of the electrodes.

The imaging techniques reported here provide the tools to characterize graphene grains and grain boundaries on all relevant length scales. These methods will be crucial both for exploring synthesis strategies to optimize grain properties and for studies, such as those described above, on the microscopic and macroscopic impact of grain structure on graphene membranes. Thus, these results represent a significant step forward in realizing the ultimate promise of atomic membranes in electronic, mechanical and energy-harvesting devices.

METHODS SUMMARY

TEM/STEM. We did ADF-STEM imaging using a NION UltraSTEM100 with imaging conditions similar to those used in ref. 21. At 60 kV, using a 33–35-mrad convergence angle, the electron probe was close to 1.3 Å in size and did not damage the graphene. Images presented in Figs 1–4 were acquired with the medium-angle annular dark-field detector with acquisition times of between 16 and 32 μs per pixel. For TEM imaging, we used a FEI Technai T12 operated at 80 kV. Acquisition times for dark-field images were 5–10 s per frame. The spatial resolution in dark-field images ranges from 1 to 10 nm and is set by the size of the objective filtering aperture, in a trade-off between real-space resolution and angular resolution in reciprocal space.

Scanning probe measurements. For AFM deflection measurements, we used a MFP3D scope from Asylum Research. We used silicon AFM probes (Multi75Al, Budget Sensors) with a resonant frequency of ~75 kHz, a force constant of ~3 N m^{-1} and a tip radius of <10 nm. All imaging was done in tapping mode. For AC-EFM measurements, a DI 4100 AFM with a signal access module was operated in lift mode with a constant probe tip voltage, $V_{tip} = 2$ V, a lift height of 10 nm and no piezo drive on the tip. An a.c. voltage of $V_0 = 1$ V was applied through the electrodes at the resonance frequency of the EFM cantilever, $f_{cant} \approx 77$ kHz. An electrostatic force drives the EFM cantilever to resonate, and the amplitude of motion is measured.

Full Methods and any associated references are available in the online version of the paper at www.nature.com/nature.

Received 23 September; accepted 29 November 2010.
Published online 5 January 2011.

1. Li, X. *et al.* Large-area synthesis of high-quality and uniform graphene films on copper foils. *Science* **324,** 1312–1314 (2009).
2. Reina, A. *et al.* Large area, few-layer graphene films on arbitrary substrates by chemical vapor deposition. *Nano Lett.* **9,** 30–35 (2009).
3. Li, X. *et al.* Graphene films with large domain size by a two-step chemical vapor deposition process. *Nano Lett.* **10,** 4328–4334 (2010).
4. Bae, S. *et al.* Roll-to-roll production of 30-inch graphene films for transparent electrodes. *Nature Nanotechnol.* **5,** 574–578 (2010).
5. Cervenka, J. & Flipse, C. F. J. Structural and electronic properties of grain boundaries in graphite: planes of periodically distributed point defects. *Phys. Rev. B* **79,** 195429 (2009).
6. Peres, N. M. R., Guinea, F. & Castro-Neto, A. H. Electronic properties of disordered two-dimensional carbon. *Phys. Rev. B* **73,** 125411 (2006).
7. Yazyev, O. V. & Louie, S. G. Electronic transport in polycrystalline graphene. *Nature Mater.* **6,** 806–809 (2010).
8. Mesaros, A., Papanikolaou, S., Flipse, C. F. J., Sadri, D. & Zaanen, J. Electronic states of graphene grain boundaries. *Phys. Rev. B* **82,** 205119 (2010).
9. Cervenka, J., Katsnelson, M. I. & Flipse, C. F. J. Room-temperature ferromagnetism in graphite driven by two-dimensional networks of point defects. *Nature Phys.* **5,** 840–844 (2009).
10. Malola, S., Hakkinen, H. & Koskinen, P. Structural, chemical, and dynamical trends in graphene grain boundaries. *Phys. Rev. B* **81,** 165447 (2010).
11. Liu, Y. & Yakobson, B. I. Cones, pringles, and grain boundary landscapes in graphene topology. *Nano Lett.* **10,** 2178–2183 (2010).
12. Grantab, R., Shenoy, V. B. & Ruoff, R. S. Anomalous strength characteristics of tilt grain boundaries in graphene. *Science* **330,** 946–948 (2010).
13. Yazyev, O. V. & Louie, S. G. Topological defects in graphene: dislocations and grain boundaries. *Phys. Rev. B* **81,** 195420 (2010).
14. Hirsch, P., Howie, A., Nicholson, R., Pashley, D. W. & Whelan, M. J. *Electron Microscopy of Thin Crystals* (Krieger, 1965).
15. Zhao, L. *et al.* The atomic-scale growth of large-area monolayer graphene on single-crystal copper substrates. Preprint at ⟨http://arxiv.org/abs/1008.3542⟩ (2010).
16. Gao, L., Guest, J. R. & Guisinger, N. P. Epitaxial graphene on Cu(111). *Nano Lett.* **10,** 3512–3516 (2010).
17. Cockayne, E. *et al.* Rotational grain boundaries in graphene. Preprint at ⟨http://arxiv.org/abs/1008.3574⟩ (2010).
18. Wofford, J. M., Nie, S., McCarty, K. F., Bartlet, N. C. & Dubon, O. D. Graphene islands on Cu foils: the interplay between shape, orientation, and defects. *Nano Lett.* **10,** 4890–4896 (2010).
19. Park, H. J., Meyer, J., Roth, S. & Skakalova, V. Growth and properties of few-layer graphene prepared by chemical vapor deposition. *Carbon* **48,** 1088–1094 (2010).
20. Regan, W. *et al.* A direct transfer of layer-area graphene. *Appl. Phys. Lett.* **96,** 113102 (2010).
21. Krivanek, O. L. *et al.* Atom-by-atom structural and chemical analysis by annular dark-field electron microscopy. *Nature* **464,** 571–574 (2010).
22. Hashimoto, A., Suenaga, K., Gloter, A., Urita, K. & Iijima, S. Direct evidence for atomic defects in graphene layers. *Nature* **430,** 870–873 (2004).
23. Meyer, J. C. *et al.* Direct imaging of lattice atoms and topological defects in graphene membranes. *Nano Lett.* **8,** 3582–3586 (2008).
24. de Villeneuve, V. W. A. *et al.* Hard sphere crystal nucleation and growth near large spherical impurities. *J. Phys. Condens. Matter* **17,** S3371–S3378 (2005).
25. Park, S., Floresca, H. C., Suh, Y. & Kim, M. J. Electron microscopy analyses of natural and highly oriented pyrolytic graphites and the mechanically exfoliated graphenes produced from them. *Carbon* **48,** 797–804 (2010).
26. Lee, C., Wei, X., Kysar, J. W. & Hone, J. Measurement of the elastic properties and intrinsic strength of monolayer graphene. *Science* **321,** 385–388 (2008).
27. Geim, A. K. & Novoselov, K. S. The rise of graphene. *Nature Mater.* **6,** 183–191 (2007).
28. Bachtold, A. *et al.* Scanned probe microscopy of electronic transport in carbon nanotubes. *Phys. Rev. Lett.* **84,** 6082–6085 (2000).
29. Van Der Zande, A. M. *et al.* Large-scale arrays of single-layer graphene resonators. *Nano Lett.* **10,** 4869–4873 (2010).
30. Thiel, S. *et al.* Electron scattering at dislocations in LaAlO3/SrTiO3 interfaces. *Phys. Rev. Lett.* **102,** 046809 (2009).

Supplementary Information is linked to the online version of the paper at www.nature.com/nature.

Acknowledgements The authors acknowledge discussions with M. Blees, J. Cha, S. Gerbode, J. Grazul, E. Kirkland, L. Fitting-Kourkoutis, O. Krivanek, S. Shi, S. Wang and H. Zhuang. This work was supported in part by the National Science Foundation through the Cornell Center for Materials Research and the Nanoscale Science and Engineering Initiative of the National Science Foundation under NSF Award EEC-0117770, 064654. Additional support was provided by the Army Research Office, CONACYT-Mexico, the Air Force Office of Scientific Research, DARPA-MTO and the MARCO Focused Research Center on Materials, Structures, and Devices. Sample fabrication was performed at the Cornell node of the National Nanofabrication Infrastructure Network, funded by the NSF. Additional facilities support was provided by the Cornell Center for Materials Research (NSF DMR-0520404 and IMR-0417392) and NYSTAR.

Author Contributions P.Y.H., C.S.R.-V. and A.M.v.d.Z. contributed equally to this work. Electron microscopy and data analysis were carried out by P.Y.H. and D.A.M., with Y.Z. contributing to initial DF-TEM. Graphene growth and sample fabrication were done by A.M.v.d.Z. and C.S.R.-V. under the supervision of P.L.M. and J.P., aided by M.P.L., S.G., W.S.W., J.W.K., J.S.A. and C.J.H. AC-EFM, mobility measurements and analysis were done by A.M.v.d.Z. and P.L.M., aided by C.S.R.-V. and J.W.K. AFM mechanical testing and analysis were done by C.S.R.-V. and J.P., aided by S.G. All authors discussed the results and implications at all stages. P.Y.H, A.M.v.d.Z., C.S.R.-V., P.L.M., J.P. and D.A.M. wrote the paper.

Author Information Reprints and permissions information is available at www.nature.com/reprints. The authors declare no competing financial interests. Readers are welcome to comment on the online version of this article at www.nature.com/nature. Correspondence and requests for materials should be addressed to D.A.M. (david.a.muller@cornell.edu).

METHODS

ADF-STEM. ADF-STEM imaging was conducted using a NION UltraSTEM100 operated at 60 kV. Imaging conditions were similar to those used in ref. 21. Using a 33–35-mrad convergence angle, our probe size was close to 1.3 Å. Because the low-voltage electron beam was below the damage threshold energy[31], the pristine graphene lattice remains stable and defect free. High electron beam doses could induce isolated bond rotations at grain boundaries (Supplementary Fig. 4) similar to those seen in ref. 32. Images presented in Figs 1–4 were acquired with the medium-angle annular dark-field detector with acquisition times of between 16 and 32 μs per pixel.

DF-TEM. TEM imaging was conducted using a FEI Technai T12 operated at 80 kV, which did not cause any apparent damage to the graphene membranes. Acquisition time for dark-field images were 5–10 s per frame. The spatial resolution in dark-field images ranges from 1 to 10 nm and is set by the size of the objective filtering aperture in a trade-off between real-space resolution and angular resolution in reciprocal space.

AC-EFM. A DI 4100 AFM with a signal access module was operated in lift mode with tip voltage $V_{tip} = 2$ V, a lift height of 10 nm and no piezo drive on the tip. An a.c. voltage $V_0 = 1$ V was applied through the electrodes at the resonance frequency of the EFM cantilever, $f_{cant} \approx 77$ kHz. An electrostatic force drives the EFM cantilever to resonate, and the amplitude of motion is measured.

AFM imaging and deflection measurements. For AFM deflection measurements, we used a MFP3D scope from Asylum Research. We used silicon AFM probes (Multi75Al, Budget Sensors) with a resonant frequency of ~75 kHz, a force constant of ~3 N m^{-1} and a tip radius of <10 nm. All imaging was done in tapping mode. Images were taken with resolutions of 512 × 512 or 1,024 × 1,024, with acquisition times of at most 10 min.

Graphene growth. We grew single-layer graphene using CVD on copper foils in three ways. Growth method A: similar to methods described in ref. 1, we annealed a 99.8% pure copper foil (Alfa Aesar #13382) at 1,000 °C at low pressure with an H_2 flow of 7 standard cubic centimetres per minute (s.c.c.m.) for 10 min. We then grew the graphene at 1,000 °C by flowing CH_4:H_2 at 150:7 s.c.c.m. for 10–15 min (varying growth time within this range did not yield noticeably different results). Samples are cooled for ~50 min while the CH_4:H_2 flow is maintained. Growth method B: this is identical to method A, except we used higher purity (99.999%) copper foil (Alfa Aesar #10950). Growth method C: we used a rapid thermal processor tube furnace with a ~4″ inner diameter (MTI Corporation). We annealed copper foil (99.8% purity) at 1,000 °C (H_2, 300 s.c.c.m.) for 30 min, and then grew the graphene at 1,000 °C (CH_4:H_2, 875:300 s.c.c.m.) for 60 min.

Samples for DF-TEM. We transferred the graphene either to commercial holey SiN TEM grids (such as PELCO Holey Silicon Nitride Support Films) with 2.5-μm-diameter holes or to Quantifoil holey carbon TEM grids to allow imaging of larger grains. Quantifoil grids are typically 10–20 nm thick, which is thin enough to allow DF-TEM imaging through the carbon support.

The fabrication for DF-TEM samples is a gentle graphene transfer method using a thin PMMA support, which produced roughly 90% coverage of TEM grid holes (that is, 90% of grid holes were uniformly covered with suspended graphene). After graphene growth on a copper foil, a thin layer of PMMA was spun onto the graphene (2% in anisole, 4,000 r.p.m. for 30 s), without a post-baking step. Copper was then etched away by floating the foil, PMMA side up, in a HCl/$FeCl_3$ copper etchant (Transene, Type 100/200). Next, the graphene and polymer support were washed by transferring them to deionized-water baths, taking care to not bring the PMMA into contact with liquids, to avoid depositing unwanted residues on the PMMA side of this layer. Finally, the PMMA–graphene layer is scooped out in pieces onto TEM grids. PMMA can be thermally decomposed[33], which is a gentler process than using liquid solvent rinses. We baked our samples in air (350 °C for 3–4 h), without the use of an argon flow, which can slow the cleaning effect substantially. This step removes the PMMA layer, leaving the graphene freely suspended in a liquid-free release process. These high-yield samples were used in DF-TEM because they provided enough clean graphene to image large numbers of grains.

Samples for ADF-STEM. Our secondary technique produced cleaner, but lower-yield, graphene using a polymer-free transfer method. This technique is similar to the methods of ref. 20, in which TEM grids are placed on top of the foil before etching and attached by dropping methanol on the grids. Our main addition to this technique was to bake the final samples in a series of annealing processes increasing in temperature. The grids were then baked in air at 350 °C for 2 h. In this method, the samples are annealed in ultrahigh vacuum by ramping the temperature to 950 °C, holding this temperature steady for 15 min and then cooling to room temperature without active cooling. This annealing is done below the graphene growth temperature, and the micrometre-scale grain structure did not change afterwards. Thus, any change that may result from annealing should be small in comparison with changes occurring during the formation of the grain boundaries. A final step was to anneal the grids at 130 °C for >8 h before transferring them in air to the TEM. Because this transfer method uses no support film for the graphene as it is transferred, this method was a comparatively low-yield transfer process with coverage of just a few per cent over the holes. The advantage to this technique over the polymer-based transfer is that it produced graphene with less surface carbon contamination—regions hundreds of nanometres wide appeared atomically clean in ADF-STEM images.

Electrically contacted samples. We fabricated top-gated graphene devices in four-point probe geometry (shown in Supplementary Fig. 11a, b, with electrodes labelled). A transferred graphene film was patterned by photolithography and a 10-s exposure to an oxygen plasma to define the graphene strips. This was followed by fabricating 1.5-nm Ti/4.5-nm Au electrodes. We patterned a top gate, to measure the charge mobility in graphene, by electron beam evaporation first of 90 nm of silicon oxide as a dielectric layer and then of a Cr/Au layer (1.5 nm/50 nm), without breaking vacuum between each evaporation.

For the EFM measurements, we fabricated electrically contacted, suspended graphene by growing single-layer graphene on copper using CVD; patterning the graphene into 3-μm-wide strips while still on the copper foil, using contact lithography; and transferring the patterned strips onto a substrate with pre-patterned gold electrodes and trenches.

31. Meyer, J. C., Chuvilin, A. & Kaiser, U. in *MC2009, Vol. 3: Materials Science* (eds Grogger, W., Hofer, F. & Polt, P.) 347–348 (Graz Univ. Technology, 2009).
32. Suenaga, K. *et al.* Imaging active topological defects in carbon nanotubes. *Nature Nanotechnol.* **2,** 358–360 (2007).
33. Jiao, L. *et al.* Creation of nanostructures with poly(methyl methacrylate)-mediated nanotransfer printing. *J. Am. Chem. Soc.* **130,** 12612–12613 (2008).